Optical and mechanical characterization of novel cobalt-based metal oxide thin films synthesized using sol-gel dip-coating method

Amun Amri, Zhong-Tao Jiang, Trevor Pryor, Chun-Yang Yin, Zonghan Xie, Nick Mondinos

PII: S0257-8972(12)00716-5
DOI: doi: 10.1016/j.surfcoat.2012.07.028
Reference: SCT 17838

To appear in: *Surface & Coatings Technology*

Received date: 18 May 2012
Accepted date: 5 July 2012

Please cite this article as: Amun Amri, Zhong-Tao Jiang, Trevor Pryor, Chun-Yang Yin, Zonghan Xie, Nick Mondinos, Optical and mechanical characterization of novel cobalt-based metal oxide thin films synthesized using sol-gel dip-coating method, *Surface & Coatings Technology* (2012), doi: 10.1016/j.surfcoat.2012.07.028

Optical and mechanical characterization of novel cobalt-based metal oxide thin films synthesized using sol-gel dip-coating method

Amun Amri[a,d], Zhong-Tao Jiang[a,*], Trevor Pryor[a], Chun-Yang Yin[b,*], Zonghan Xie[c], Nick Mondinos[a]

[a]*School of Engineering and Energy, Murdoch University, Murdoch, 6150 WA, Australia*

[b]*School of Chemical and Mathematical Sciences, Murdoch University, Murdoch, 6150 WA, Australia.*

[c]*School of Mechanical Engineering, University of Adelaide, SA 5005, Australia*

[d]*Department of Chemical Engineering, Riau University, Pekanbaru, Indonesia*

*Corresponding author. Tel.: +618 9360 2867; Email address: z.jiang@murdoch.edu.au

* Tel.: +614 3140 9216; Email address: c.yin@murdoch.edu.au; yinyang@streamyx.com

Abstract

New cobalt-based metal oxide thin films ($M_xCo_yO_z$ with M = Mn, Cu, Ni) have been deposited on commercial aluminium and glass substrates using sol-gel dip-coating method. The as-deposited films were characterized by a wide range of complementary techniques including X-ray diffraction (XRD), scanning electron microscopy (SEM), atomic force microscopy (AFM), X-ray photoelectron spectroscopy (XPS), Spectrophotometry and Nanoindentation techniques. A light absorption study for coatings on glass substrates within a wavelength range of 300-1100 nm was also conducted. Topographical and morphological investigations showed the presence of nano-sized, grain-like particles in the copper-cobalt oxide coatings, which consequently had the roughest surface among the three coatings. All coatings on glass substrate exhibited higher absorption of ultraviolet (UV) light compared to visible light, while coatings on aluminium substrate generally had low reflectance (< 50 %) of UV light, moderate reflectance (< 80 %) of visible light and high reflectance (up to 100 %) of infrared light. Implications of optical properties as a function of film thickness controlled by dip-heating cycles were discussed. The elastic modulus (*E*) and hardness *(H)* of thin film samples compared with standalone commercial aluminium substrate were also measured.

Keywords*: Cobalt-based metal oxides; sol-gel dip-coating; optical and mechanical properties; X-ray photoelectron spectroscopy; nanoindentation*

1. Introduction

Cobalt-based metal oxides ($M_xCo_yO_z$ with M = Mn, Cu, Ni and derivatives) are highly versatile functional materials, which have found widespread utilization in a variety of high-tech applications. These include applications in catalytic processes [1-4], electrochemistry [5-7], batteries and memory devices [8-10], solid oxide fuel cells [11, 12] and electronics [13]. Manganese-cobalt oxides ($Mn_xCo_yO_z$) are a group of widely investigated metal oxides with particular emphasis on the influence of the synthesis conditions on the oxidation states and cation distribution in the cubic and tetragonal phases as typically described in the Mn-Co-O system [14]. The physicochemical properties of manganese-cobalt oxide are greatly affected by the synthesis temperature, crystal structure, anion oxidation states and composition [15]. Electrical properties of manganese-cobalt oxide have also been investigated by Bordeneuve and co-researchers [16]. Likewise, there have been numerous studies conducted to characterize the physicochemical, magnetic, conductivity, electrochemical and thermal properties of copper-cobalt oxides [1, 17-20] as well as nickel-cobalt oxides [7, 21, 22]. Nickel-cobalt oxides have been reported to possess improved electronic conductivity properties, i.e., at least two orders of magnitude higher than those of nickel or cobalt oxides [13].

An area of application of which these cobalt-based oxides are comparatively less studied is optical or solar-based coating whereby optical performance of a surface can be manipulated by depositing thin films with varying thicknesses and reflective indices. For example, Kaluza and co-researchers [23] synthesized $CuCoMnO_x$ spinel coatings using dip-coating method which showed good potential as solar absorber coatings. In a more recent study, Bayon *et al.* [24] reported deposition of CuMn-spinel layers on aluminium substrate as solar selective absorbers using a similar sol-gel method. Incidentally, there are certainly many knowledge gaps that need to be filled in terms of fundamental surface characteristics of these thin films especially in regard to their morphologies, binding states of metal oxides and mechanical

strengths. A technical understanding of these characteristics is an essential component in the smart design and engineering context of thin film coatings for optical applications.

In this study, manganese-, copper- and nickel-cobalt oxides thin film coatings on commercial aluminium substrates have been synthesized using the sol-gel dip-coating method. The sol-gel process is a soft chemistry method whereby the precursors are often in a form of colloidal solution that ultimately 'transforms' into an extensive network of either discrete or continuously-linked molecules. In our case, it was selected due to its inherently simple and safe characteristics in which solid-state synthesis could be accomplished at relatively low temperatures [17, 25]. In this paper, we analyze the relationships between the surface, optical and mechanical characteristics of the synthesized cobalt-based oxides film coatings by employing X-ray diffraction (XRD), scanning electron microscopy (SEM), atomic force microscopy (AFM), X-ray photoelectron spectroscopy (XPS), spectrophotometry and nanoindentation techniques. Light absorption analysis for coatings on glass substrate within a wavelength range of 300-1100 nm was also conducted. The comprehensive and novel surface-based data with respect to thorough XPS and nanoindentation analyses conducted in this study are significant as they affords a novel understanding of the morphological and binding states/conditions of the aforesaid cobalt-based oxides which complement the existing knowledge on other mixed metal oxides. The motivation behind our study is clear; detailed findings on surface analyses can be utilized to aid the surface engineering designs of tuneable thin film metal oxides for a myriad of industrial applications such as optical coatings and solar-selective absorbers.

2. Experimental

2.1. Preparation of thin film coatings

Cobalt (II) chloride ($CoCl_2.6H_2O$, APS Chemical, > 99 %), anhydrous manganese (II) acetate ($C_4H_6MnO_4$, Alfa Aesar, > 98 %), copper (II) acetate monohydrate ($Cu(OOCCH_3)_2.H_2O$, Alfa Aesar, 98 %), nickel (II) acetate tetrahydrate ($Ni(OOCCH_3)_2.4H_2O$, Alfa Aesar, 98 %), propionic acid (C_2H_5COOH, Chem Supply, 99 %) and absolute ethanol (Merck) were used as received.

Two types of substrates were used, namely, glass microscope slides and commercial highly reflecting aluminium (Anofol). The glass substrates were used only for optical absorptance studies and had a glass transition temperature over 1200 ºC. The glass substrates were rinsed using distilled water then ultrasonically cleaned in acetone for 15 minutes and dried in a vacuum oven at 60^o C to remove residual moisture. The aluminium substrates were cleaned using an etching solution to minimize the alumina layer. The etching solution was produced by dissolving chromium (VI) oxide (35 g) and 20 mL of 85% phosphoric acid in 1L of distilled water. The aluminium substrates were placed in the hot etching solution (85°C) for 10 minutes and subsequently rinsed in hot distilled water. This was followed by a flush of distilled water and drying in a nitrogen stream.

Cobalt chloride ($CoCl_2.6H_2O$, 0.15 M) and manganese acetate ($C_4H_6MnO_4$, 0.15 M) were mixed using absolute ethanol. Propionic acid (C_2H_5COOH) was then added to the solution as complexing agent and stirred for 2 hours. The resulting solution was then used for thin film deposition on aluminium or glass substrates using dip-coating at withdrawal rate of 60 mm/min and subsequently heated at 150°C for 10 minutes. Humidity was maintained at less than 55% so that a relatively smooth and even film could be produced. The adhesion of mixed metal oxide film on the substrate was immediate (*ca* 10 seconds) during the dipping process. Manganese-cobalt thin films with varying thicknesses were prepared by repeating the dip-

heating cycle two or six times before annealing in oven at temperature 500 °C for 1 hour to remove volatiles. An analogous procedure was used to prepare the copper-cobalt and nickel-cobalt mixed metal oxides thin films.

2.2. Characterizations

Mineralogical characteristics of the thin films were analyzed using X-ray diffractometry (XRD) using a GBC EMMA diffractometer with CuK_{α} radiation and operating with a step size of 0.01^{o}. Surface topographic images of the thin films were obtained using a commercial atomic force microscope (AFM) (Ntegra Prima, NT-MDT Co., Moscow, Russia) in semi-conduct mode. The thin film samples were fixed on adhesive tape before AFM scans were conducted. The probe used for the imaging contained a tetrahedral tip with a height of 14-16 μm and a typical curvature radius of 6 nm. The tip was mounted on a rectangular single crystal silicon (N-type, antimony doped) cantilever with a thickness of 2 μm, a resonant frequency of 140-390 kHz and a force constant of 3.1-37.6 N/m.

The surface morphologies of the film samples were examined using a PHILLIPS XL 20 scanning electron microscopy (SEM) and field emission scanning electron microscopy (FESEM) (Zeiss Neon 40EsB). For FESEM, the sample was mounted on the substrate holder using carbon tape and sputter-coated with platinum to reduce charging effects before analysis. InLens detectors were used to obtain FESEM images at various magnifications at 5 kV. Absorption spectra (for coatings on glass substrate) within the wavelength range of 300-1100 nm were recorded using a Varian CARY 50 Bio UV−vis Spectrophotometer while solar absorptance was calculated based on the AM1.5 solar spectrum standard using the hemispherical reflectance recorded from 300 to 2700 nm using a UV-Vis-NIR Jasco V-670 double beam spectrophotometer with 60 mm integrating sphere.

The atomic percentages and surface bonding structures of samples were probed by X-ray photoelectron spectroscopy (XPS) (Kratos Axis Ultra XPS spectrometer, Manchester, UK) with Mg K_α radiation (hv = 1253.6 eV). The samples were mounted, using double-sided Cu sticky tape, horizontally on the holder and normal to the electrostatic lens. The vacuum pressure of the analyzer chamber was better than 10^{-9} Torr. The voltage and emission current of the X-ray source were held at 12 kV and 12 mA, respectively. Initial survey scans used a pass energy of 80 eV. To ensure high resolution and good sensitivity for the features of interests, pass energy of 10 eV was used. The XPS spectra energy scale was calibrated using Cu 2p (932.67 eV), Ag 3d (368.27 eV), C 1s (284.8 eV; hydrocarbon: C-H) and Au 4f (83.98 eV). The electrostatic lens mode and analyzer entrance of the XPS instrument were selected using the Hybrid and Slot mode (Iris = 0.6 and Aperture = 49), respectively. Charge neutralization was employed during the XPS measurements. The CASA XPS (V.2.3.15) software [26] was utilized for quantification analysis with Shirley background subtraction.

A nanoindentation workstation (Ultra-Micro Indentation System 2000, CSIRO, Sydney, Australia) equipped with a Berkovich indenter was used to determine the mechanical properties of the films [27]. The procedure can be briefly described as follows: The area function of the indenter tips was calibrated using a standard fused silica specimen. Nanoindentation was conducted under load control with a maximum load of 0.5 mN. For each test, 10 incremental and 10 decremental steps were used. The maximum penetration depth during the tests was found to be <10% of the film thickness, which ensured that only the film properties were measured. Twenty indentations were performed for each sample.

3. Results and Discussion

3.1. XRD analysis

Fig. 1a shows the XRD patterns of the prepared manganese-cobalt (i), copper-cobalt (ii) and nickel-cobalt (iii) thin film coatings (6 dip-heating cycles) on aluminium substrate and standalone heated and unheated aluminium substrate (iv and v), respectively. The XRD patterns of the samples made with a 2 dip-heating cycle indicate marginal difference from the aluminium substrate patterns (10^o to 40^o range) and as such only samples from the 6 dip-heating cycle are considered for analysis.

The XRD pattern of the heated standalone substrate (Fig. 1a.(iv)) shows peaks at approximately 45^o (95 65^o (100%) and 78^o (19%) where the percentages in brackets are with respect to the observed main intensity peak. The XRD pattern of the unheated standalone substrate (Fig. 1a.(v)) has two main peaks at approximately 65^o and 78^o and a very small intensity peak (0.4%) at approximately 45^o. Peaks from the $M_xCo_yO_z$ (M = Cu, Mn, Ni) films are very hard to resolve in the 2θ ranges observed for the substrates. Some peaks with intensities of approximately 0.3%-0.5% of the main intensity peak of the substrates shown in Fig. 1b (i)–(iii) are, when compared with the observed Al substrate plots of Fig.1b (iv) and (v), interpreted as due to $M_xCo_yO_z$ (M = Cu, Mn, Ni) phases. The XPS analysis indicates the presence of oxygen, cobalt and metal (Cu, Ni or Mn) atoms on the surface of the aluminium substrates. It is difficult to make conclusions on the stoichiometric formulation of the metal-oxide phases present or on their crystallinity but it should be noted that poor crystallinity of $M_xCo_yO_z$ (with M = Mn, Cu, Ni) synthesized by the sol-gel method has been reported by other researchers [17, 28, 29].

3.2. Surface topography and morphology

AFM images indicate that the manganese-cobalt and nickel-cobalt coatings are smoother than copper-cobalt coatings (Fig. 2). The peaks and valleys (exhibited in the form of contours) provide a quantitative indication of the surface roughness and absorptancy of the coatings. In regard to surface roughness, the arithmetic average height deviation (Sa) values for manganese-cobalt, nickel-cobalt and copper-cobalt are 17.61, 8.42 and 20.63 nm, respectively. SEM and FESEM analysis corroborate this observation whereby the morphology of a copper-cobalt coating shows the presence of nano-sized grain-like particles (Fig. 3). With close examination of these micrographs, the morphology of the grain-like particles is more obvious with sizes ranging from 20 to 100 nm which are embedded within pores/trenches. These grain-like particles were also reported by Marsan and co-researchers [30] for their porous copper-cobalt oxide $Cu_xCo_{3-x}O_4$ layers. The thickness of film coating can be approximated from the Peak-to-peak (Sy) parameter from AFM analysis result. Based on peak-to-peak values, the manganese-cobalt, copper-cobalt and nickel-cobalt thin films coatings are estimated to have the thickness per dipping of around 104, 221 and 172 nm, respectively. The observation that copper-cobalt coating has the highest thickness is consistent with the presence of sharp peaks as shown in the AFM image.

3.3. XPS analysis

Fig.4. shows the C1s, O1s and Mn2p, Cu2p, Ni2p, Co2p XPS spectra of manganese-cobalt, copper-cobalt and nickel-cobalt thin film coatings. The binding energies (BE) of each component are evaluated by using a Gaussian-Lorentzian fit. The decoupling of the C1s spectra from all three samples shows four carbon bonding states, *i.e.*, (1) C–H and C–C (284.7 – 284.9 eV); (2) C-O (286.4-286.6 eV); (3) O=C-O (288.2 288.5 eV); and (4) C-metal (*i.e.*, metal carbide) (281.7 – 283.9 eV). The C-metal bond of copper-cobalt coating consists only

of cobalt carbide (C-Co) bonding. This is understandable as carbon is not miscible nor reactive to the copper [31]. The manganese carbide binding energy is very rarely found in the literature. However, the binding energy of transition metals in carbides is normally in region of around 281-284 eV, and it can shift by 0.5-0.7 eV depending on the chemical environment of the transition metal [32]. Ioffe et al. [32] proposed the binding energy of manganese carbide (C-Mn) to be 282.5 eV. Our C 1s XPS spectrum shows that a very strong component located at around 281.7 (Fig 4 (a1)) is most likely assigned as manganese carbide due to the high ratio of Mn/Co in the manganese-cobalt thin film as seen in Table 1. The presence of other carbon states in the bonding energy above 285.0 eV in all coatings could be due to the reaction or adsorption of the propionic acid derivatives (propionic acid from the solution preparation).

The decoupling of the O1s photoelectron spectrum shows three components, namely, (1) lattice O^{2-} (O-metal bonds) (529.4 – 529.8 eV) [1, 17, 33]; (2) surface oxygen, including adsorbed oxygen species, as hydroxyl (OH), carbonate group, *etc*. (531.1 – 531.2 eV) [1, 17]; and (3) subsurface O^{-} species (531.9 – 532.2 eV) [34, 35]. For the manganese-cobalt coating, the two components representing Co-O and Mn-O binding energy are separated by 0.4 eV (Fig. 4.b1.) while for the other two coatings, the Co-O and Cu-O/Ni-O binding energy peaks overlap. The manganese-cobalt coating does not have subsurface (bulk structure near the surface) oxygen (O^{-}). The subsurface oxygen ions have lower electron density than the O^{2-} ions. They can be associated with sites where the coordination number of oxygen ions is smaller than in a regular site, with higher metal oxide bonds [34].

Generally, each of the Mn 2p, Cu 2p, Ni 2p and Co 2p XPS spectra (Fig 4. c1-c3 and Fig 4. d1-d3) has two main peaks representing $2p_{3/2}$ and $2p_{1/2}$. Based on their binding energy, these main peaks indicate that the oxide states of Mn, Cu, Ni or Co are present in the surface coating [36]. Comparison of the Mn 2p spectrum with the Co 2p spectrum (Fig. 4 c1-d1) suggests that the manganese-cobalt surface coating has much higher manganese concentration

than cobalt, while the copper-cobalt and nickel-cobalt surface coating have a comparable concentration between copper or nickel and cobalt, respectively (Fig. 4.c2-d2 and Fig. 4.c3-d3). Table 1 shows the metal compositions in the surface coatings. The observed higher concentration of Mn in the manganese-cobalt system can be explained based on the nature of the surface cobalt itself where cobalt tends to leave more surface cation positions empty than manganese resulting in much lower cobalt concentration on the sample surface [37].

Gautier et al. [1] argued that the low intensity satellites of the Co 2p spectra in the copper-cobalt surface system indicated that the Co ions were present in a spinel-type lattice arrangement, while the binding energy of Co $2p_{3/2}$ and $2p_{1/2}$ corresponded to the octahedral diamagnetic Co(III) ions existing in a low-spin state. They further argued that the non-satellite peaks in Cu 2p spectra which had a binding energy difference of around 20 eV could be attributed to Cu(II) ions whereas the strong satellites indicated Cu^{2+} as in CuO. If cobalt was present as diamagnetic Co^{III} ions and copper was present as Cu^{2+} ions, then the oxide could be represented by the $Cu^{2+}Co_2^{III}O_4$ formula [1]. All of these characteristics mentioned by Gautier et al. [1] match the results seen in Fig. 4.c2-d2.

The peak of Ni $2p_{3/2}$ in the nickel-cobalt coating (Fig. 4. c3) represents two oxidation states: firstly, the Ni(II) ions present on the surface as NiO, and secondly the Ni(II) ions or Ni(III) species present on the surface as $Ni(OH)_2$, while the satellite at around 862 eV indicates the presence of paramagnetic Ni ions [38]. Regarding the Co-2p curve in the nickel-cobalt sample (Fig. 4. d3), the low satellite band structure points to a surface depletion of paramagnetic Co(II) ions [38].

3.4. Optical properties

The optical properties of the thin film coatings are evaluated on the basis of absorptance (α) and reflectance (R). Absorptance is defined as a weighted fraction between absorbed radiation and incoming radiation [39]. The absorptance of a thin film on a substrate can be

determined in terms of reflectance as described by Duffie and Beckman [39]. Low spectral reflectance indicates high absorptance and *vice versa*. To the best of our knowledge, only a few previous studies on the optical properties of cobalt-based metal oxides ($M_xCo_yO_z$ with M = Mn, Cu, Ni) thin film coatings have been carried out [1, 22, 40, 41].

Absorption spectra for all thin film coatings on glass substrates within a wavelength range of 300-1100 nm are shown in Fig. 5. It is obvious that all coatings show higher absorption of ultraviolet (UV) light compared to visible light with gradual increases in absorption from the infrared (> 740 nm) to the UV range (< 400 nm). It is also clear that the nickel-cobalt thin film has the lowest absorptive capability among all the films, albeit the increase of dip-heating cycles increases their absorptive capability significantly. This implies that the thickness of the nickel-cobalt layer plays a crucial role in UV and visible light absorption properties, *i.e.*, this effect is even more pronounced in nickel-cobalt compared to manganese-cobalt and copper-cobalt.

The absorption spectra of manganese-cobalt film (Fig. 5.a,b) show a broad absorption band at around 570-750 nm with maximum at $\lambda \approx 700$ nm. We postulate that this band corresponds to a metal-metal charge transfer band between cobalt ions which indicates the formation of segregated Co_3O_4 [1] in the manganese-cobalt spinel surface. The copper-cobalt film spectra (Fig. 5.c,d) seem to indicate that practically no band is detected. This is attributed to the doping of Cu^{2+} ions into the lattice which causes replacement at octahedral and tetrahedral Co sites, thus removing the orbital degeneracy and adding new orbital energy levels [1]. This postulate can also be extended for no-band detection in nickel-cobalt film (Fig. 5. e,f) in terms of the presence of Ni^{2+} ions.

Reflectance spectra of all thin film coating samples on aluminium substrates, together with the corresponding solar absorptance values, are shown in Fig. 6. Aluminium is selected as the substrate for reflectance analysis because it is highly reflective and inexpensive. The prepared coatings generally have low reflectance (< 50 %) of UV light, moderate reflectance (< 80 %)

of visible light and high reflectance (up to 100 %) of infrared light. The copper-cobalt (with 6 dip-heating cycles) sample represents an anomaly amongst all the thin films because of its rather low reflectance value which contributes to its comparatively high absorptance value of 71.3%. Inspection of Figs. 5 and 6 reveals that the choice of substrate has a substantial influence on the absorptive property of the copper-cobalt film. It can be construed that absorptive property of copper-cobalt layer is affected by both its thickness and the composition of the substrate. The copper-cobalt thin film on an aluminium substrate experiences an increase of 29.5 % in absorptance with a three-fold increase in dip-heating cycles.

The discrepancies in the absorptance values of the samples can be explained by close examination of the morphology and roughness of the deposited layers. Rincon and co-researchers [42] argued that a rough surface reduced reflection of incident radiation at the film surface, while surface pores contributed to lower refractive index. As such, this boosts the absorptance due to the interaction and relaxation mechanism in the absorber as well as multiple reflections and resonant scattering in the pores (*ibid*). The observation that the copper-cobalt film is rougher and more porous than the other samples in our SEM, FESEM and AFM analyses corroborates our absorptance and reflectance results. Marsan and co-researchers [30] suggested that the rougher morphology of copper-cobalt oxide surface was attributed to higher evolution of gas volumes (NO_2, O_2) during the decomposition of the concentrated nitrate coating. In line with their analysis, the roughness of our copper-cobalt surface is possibly attributed to evolution of O_2 from high temperature decomposition of copper and/or cobalt oxides which ultimately form the $Cu_xCo_yO_z$ system [5, 43].

3.5. Nanoindentation

The values of elastic modulus (*E*) and hardness *(H)* of thin films compared with those of standalone commercial aluminium substrate are presented in Fig. 7, while their load-

displacement curves are shown in Fig. 8. There are marginal differences in terms of *E* and *H* between the three thin films albeit all films exhibit significantly lower *E* (by 44-50 %) and hardness (by 68-83 %) compared to the aluminium substrate. Among the three thin films tested, nickel-cobalt film exhibits the highest average elastic modulus while the other two have similar values of elastic modulus (*i.e*. similar stiffness). In addition, the nickel-cobalt thin film sample is the hardest among the three films. There is an observed difference in average hardness (*ca* 30 MPa) between nickel-cobalt and copper-cobalt films. The representative load-displacement curves in Fig. 8 show the responses of the three thin films to increasing mechanical loadings, and indicate a trend that reflects the *E* and *H* results. The level of resistance to deformation increases via the following sequence: manganese-cobalt, copper-cobalt and nickel-cobalt.

As far as we are aware, no mechanical properties have been measured on this type of films, though such properties are important to their functions and durability. Nonetheless, it is deemed appropriate that previous reported mechanical characteristics (values) for other coatings be noted as references/benchmarks for our nanoindentation study. For example, the SiO_2/TiO_2/ORMOSIL composite for optical coating synthesized by similar sol-gel method (annealing at 500 °C) has a hardness higher than the present film coatings by *ca* 2 GPa [44], though the latter have higher *E* values (by approximately 40 GPa). Chan et al. [45] investigated the thermal, optical and mechanical properties of sol-gel-derived silica-based coatings on polyester substrates incorporated with organic and transition metal oxides components. Nanoindentation analysis revealed that their coatings have a surface hardness up to 2.5 GPa and *E* values up to 13.6 GPa, which is approximately an order of magnitude higher than that of the plastic surface. They also reported that the addition of transition metal oxides led to a coating with reduced hardness due to the low density structure resulting from the rapid condensation reactions of catalytic effect of transition metal oxides [45].

4. Conclusions

Cobalt-based metal oxide thin films have been successfully deposited on commercially available aluminium substrates as thin film coatings in $Mn_xCo_yO_z$, $Cu_xCo_yO_z$ and $Ni_xCo_yO_z$ mineralogical forms using sol-gel dip-coating method. The distinctive morphological (nano-sized, grain-like particles) and optical features of the copper-cobalt coatings imply good prospects for future application as a solar absorber coating material, though they still need further engineering to improve optimal performance. All three coatings exhibit higher absorption of UV light compared to visible light with gradual increases in absorption from the infrared (> 740 nm) to the UV range (< 400 nm). The nickel-cobalt film has the lowest absorptive capability among all the films, although the increase of dip-heating cycles increases their absorptive capability considerably. In terms of reflectance, the films generally have low reflectance (< 50 %) of UV light, moderate reflectance (< 80 %) of visible light and high reflectance (up to 100 %) of infrared light. Our findings can be used to aid the engineering design of highly tuneable thin film metal oxides for numerous industrial applications, such as optical coatings and solar-selective absorbers. Our obtained nanoindentation data infer that the mechanical properties of the films are generally favorable and can be applied in industrial conditions. Lastly, comprehensive surface data such as XPS descriptions reported here for manganese- and nickel-cobalt coatings may be useful as the basis for engineering design of thin film coatings for other important industrial applications.

Acknowledgment

Amun Amri gratefully acknowledges the Indonesian government for providing a Ph.D. scholarship. The authors acknowledge Ken Seymour, Dr Gerrard Eddy Poinern (Murdoch Applied Nanotechnology Research Group) and Hua Guo (Edith Cowan University) for their assistance.

References

[1] J.L. Gautier, E. Trollund, E. Ríos, P. Nkeng, G. Poillerat, Journal of Electroanalytical Chemistry, 428 (1997) 47-56.
[2] B. Cui, H. Lin, J.-B. Li, X. Li, J. Yang, J. Tao, Advanced Functional Materials, 18 (2008) 1440-1447.
[3] M.A. Carreon, V.V. Guliants, L. Yuan, A.R. Hughett, A. Dozier, G.A. Seisenbaeva, V.G. Kessler, European Journal of Inorganic Chemistry, 2006 (2006) 4983-4988.
[4] T. Nissinen, M. Leskela, M. Gasik, J. Lamminen, Thermochimica Acta, 427 (2005) 155-161.
[5] J.L. Gautier, E. Rios, M. Gracia, J.F. Marco, J.R. Gancedo, Thin Solid Films, 311 (1997) 51-57.
[6] D. Klissurski, E. Uzunova, Chemistry of Materials, 3 (1991) 1060-1063.
[7] M. Guene, A.A. Diagne, M. Fall, M.M. Dieng, G. Poillerat, Bulletin of the Chemical Society of Ethiopia, 21 (2007) 255-262.
[8] S. Guillemet-Fritsch, C. Tenailleau, H. Bordeneuve, A. Rousset, Advances in Science and Technology, 67 (2010) 143-148.
[9] A.V. Chadwick, S.L.P. Savin, S. Fiddy, R. Alcántara, D. Fernández Lisbona, P. Lavela, G.F. Ortiz, J.L. Tirado, The Journal of Physical Chemistry C, 111 (2007) 4636-4642.
[10] R. Alcántara, M. Jaraba, P. Lavela, J.L. Tirado, Chemistry of Materials, 14 (2002) 2847-2848.
[11] Z. Yang, G. Xia, S.P. Simner, J.W. Stevenson, Journal of The Electrochemical Society, 152 (2005) A1896-A1901.
[12] A. Balland, P. Gannon, M. Deibert, S. Chevalier, G. Caboche, S. Fontana, Surface and Coatings Technology, 203 (2009) 3291-3296.
[13] T.-Y. Wei, C.-H. Chen, H.-C. Chien, S.-Y. Lu, C.-C. Hu, Advanced Materials, 22 (2010) 347-351.
[14] E. Vila, R.M. Rojas, J.L. Martin de Vidales, O. Garcia-Martinez, Chemistry of Materials, 8 (1996) 1078-1083.
[15] H.T. Zhang, X.H. Chen, Nanotechnology, 17 (2006) 1384.
[16] H. Bordeneuve, C. Tenailleau, S. Guillemet-Fritsch, R. Smith, E. Suard, A. Rousset, Solid State Sciences, 12 (2010) 379-386.
[17] M. De Koninck, S.-C. Poirier, B. Marsan, Journal of The Electrochemical Society, 153 (2006) A2103-A2110.
[18] R.N. Singh, J.P. Pandey, N.K. Singh, B. Lal, P. Chartier, J.F. Koenig, Electrochimica Acta, 45 (2000) 1911-1919.
[19] M. Hamid, A.A. Tahir, M. Mazhar, K.C. Molloy, G. Kociok-Köhn, Inorganic Chemistry Communications, 11 (2008) 1159-1161.

[20] W.M. Shaheen, A.A. Ali, Materials Research Bulletin, 36 (2001) 1703-1716.
[21] J.G. Kim, D.L. Pugmire, D. Battaglia, M.A. Langell, Applied Surface Science, 165 (2000) 70-84.
[22] C.F. Windisch Jr, G.J. Exarhos, K.F. Ferris, M.H. Engelhard, D.C. Stewart, Thin Solid Films, 398-399 (2001) 45-52.
[23] L. Kaluza, B. Orel, G. Drazic, M. Kohl, Solar Energy Materials and Solar Cells, 70 (2001) 187-201.
[24] R. Bayón, G. San Vicente, C. Maffiotte, Á. Morales, Renewable Energy, 33 (2008) 348-353.
[25] R. Mechiakh, N.B. Sedrine, J.B. Naceur, R. Chtourou, Surface and Coatings Technology, 206 (2011) 243-249.
[26] N. Fairley, CasaXPS Manual 2.3.15 Spectroscopy, Casa Software Ltd, Teignmouth-Devon, 2009.
[27] W.C. Oliver, G.M. Pharr, Journal of Materials Research, 19 (2004) 3-20.
[28] A. Restovic, E. Rios, S. Barbato, J. Ortiz, J.L. Gautier, Journal of Electroanalytical Chemistry, 522 (2002) 141-151.
[29] M. El Baydi, S.K. Tiwari, R.N. Singh, J.-L. Rehspringer, P. Chartier, J.F. Koenig, G. Poillerat, Journal of Solid State Chemistry, 116 (1995) 157-169.
[30] B. Marsan, N. Fradette, G. Beaudoin, Journal of The Electrochemical Society, 139 (1992) 1889-1896.
[31] G. Speranza, L. Minati, M. Anderle, Journal of Applied Physics, 102 (2007) 043504-043507.
[32] L.M. Ioffe, P. Bosch, T. Viveros, H. Sanchez, Y.G. Borodko, Materials Chemistry and Physics, 51 (1997) 269-275.
[33] F. Hao, J. Zhong, P.-L. Liu, K.-Y. You, C. Wei, H.-J. Liu, H.-A. Luo, Journal of Molecular Catalysis A: Chemical, 351 (2011) 210-216.
[34] J.-C. Dupin, D. Gonbeau, P. Vinatier, A. Levasseur, Physical Chemistry Chemical Physics, 2 (2000) 1319-1324.
[35] S. Royer, A. Van Neste, R. Davidson, S. Mcintyre, S. Kaliaguine, Industrial & engineering chemistry research, 43 (2004) 5670-5680.
[36] J.F. Moulder, W.F. Stickle, P.E. Sobol, K.D. Bomben, Handbook of X-ray Photoelectron Spectroscopy: A Reference Book of Standard Spectra for Indentation and Interpretation of XPS Data, Perkin Elmer Corporation, Minnesota-USA, 1992.
[37] D.G. Klissurski, E.L. Uzunova, Applied Surface Science, 214 (2003) 370-374.
[38] A.C. Tavares, M.I. da Silva Pereira, M.H. Mendonça, M.R. Nunes, F.M. Costa, C.M. Sá, Journal of Electroanalytical Chemistry, 449 (1998) 91-100.
[39] J.A. Duffie, W.A. Beckman, Solar Engineering of Thermal Processes, third ed., John Wiley & Sons Inc., New Jersey, 2006.
[40] J.C.F. Windisch, K.F. Ferris, G.J. Exarhos, in: The 47th international symposium: Vacuum, thin films, surfaces/interfaces, and processing NAN06, AVS, Boston, Massachusetts (USA), 2001, pp. 1647-1651.
[41] P. Nkeng, G. Poillerat, J.F. Koenig, P. Chartier, B. Lefez, J. Lopitaux, M. Lenglet, Journal of The Electrochemical Society, 142 (1995) 1777-1783.
[42] M.E. Rincón, J.D. Molina, M. Sánchez, C. Arancibia, E. García, Solar Energy Materials and Solar Cells, 91 (2007) 1421-1425.
[43] K. Petrov, L. Markov, Journal of Materials Science, 20 (1985) 1211-1214.
[44] W. Que, Z. Sun, Y. Zhou, Y.L. Lam, S.D. Cheng, Y.C. Chan, C.H. Kam, Materials Letters, 42 (2000) 326-330.
[45] C.M. Chan, G.Z. Cao, H. Fong, M. Sarikaya, T. Robinson, L. Nelson, Journal of Materials Research, 15 (2000) 148-154.

Table 1. Metal composition analysis of film coatings using XPS.

Coating	Atomic concentration (%)	Atomic ratio
Manganese-cobalt	Mn=14.93% Co=2.23%	Mn:Co = 6.7:1
Copper-cobalt	Cu =5.09% Co=10.62%	Cu:Co = 0.5:1
Nickel-cobalt	Ni =9.4% Co=7.84%	Ni:Co = 1.2:1

List of Figure Captions

Fig. 1. (a) XRD patterns of the prepared manganese-cobalt (i), copper-cobalt (ii) and nickel-cobalt (iii) thin film coatings (6 dip-heating cycles) on aluminium substrate and standalone heated and unheated aluminium substrate (iv and v) respectively. (b) Expanded XRD pattern region from 10^{o} to 40^{o} (intensity of observed peaks are 0.3%-0.5% of maximum intensity peak of substrate from Fig.1(a)).

Fig. 2. AFM images of the a) manganese-cobalt; b) copper-cobalt; and c) nickel-cobalt thin film coatings (6 dip-heating cycles).

Fig. 3. SEM micrographs of the a) manganese-cobalt; b) copper-cobalt; and c) nickel-cobalt thin film coatings. FESEM micrograph for copper-cobalt indicates the presence of nano-sized grain-like particles (6 dip-heating cycles).

Fig. 4. XPS spectra of manganese-cobalt, copper-cobalt and nickel-cobalt thin film coatings. Dashed lines correspond to fit envelopes, while wavy lines correspond to data curves.

Fig. 5. Absorption spectra of thin film coatings on the glass substrates. Absorption due to glass substrate was eliminated from the spectra.

Fig. 6. Reflectance spectra of thin film coatings on aluminium substrates with corresponding solar absorptance (α) values.

Fig. 7. Elastic modulus and hardness of the thin films measured using the nanoindentation.

Fig. 8. Typical load-displacement curves of the thin films measured using the nanoindentation.

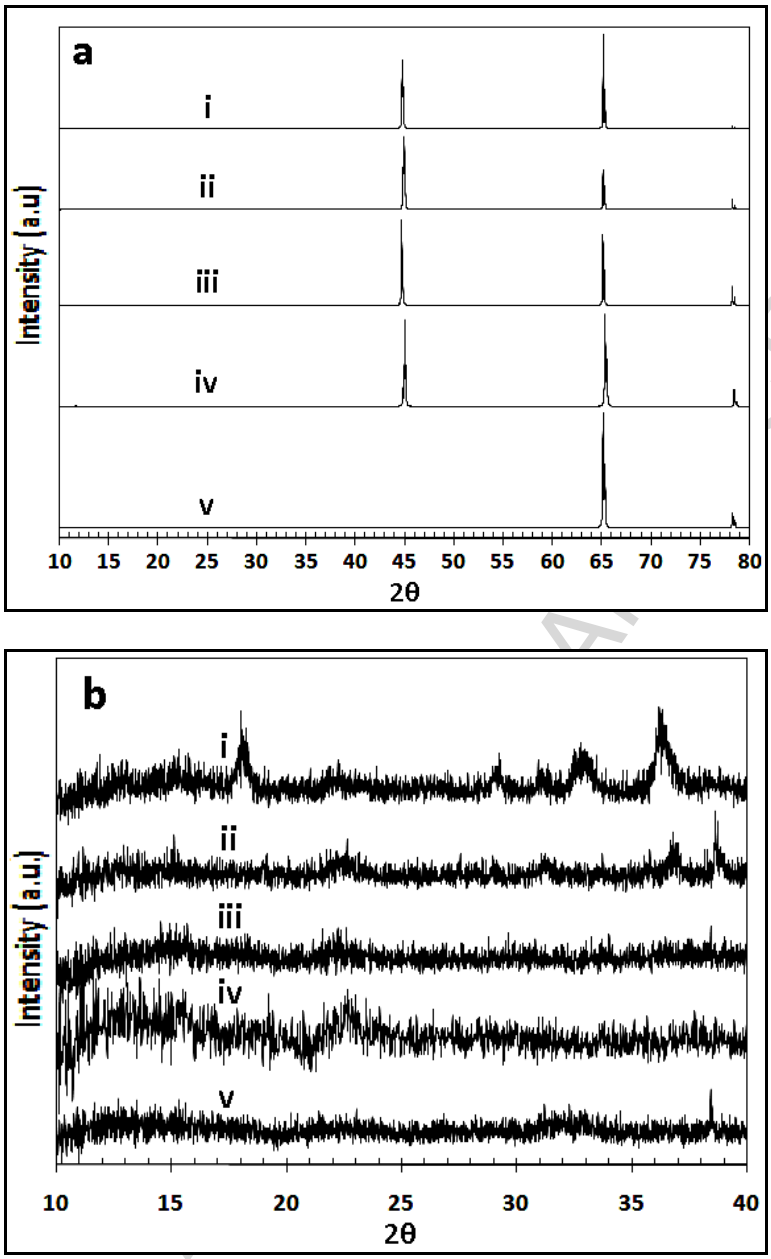

Fig. 1.

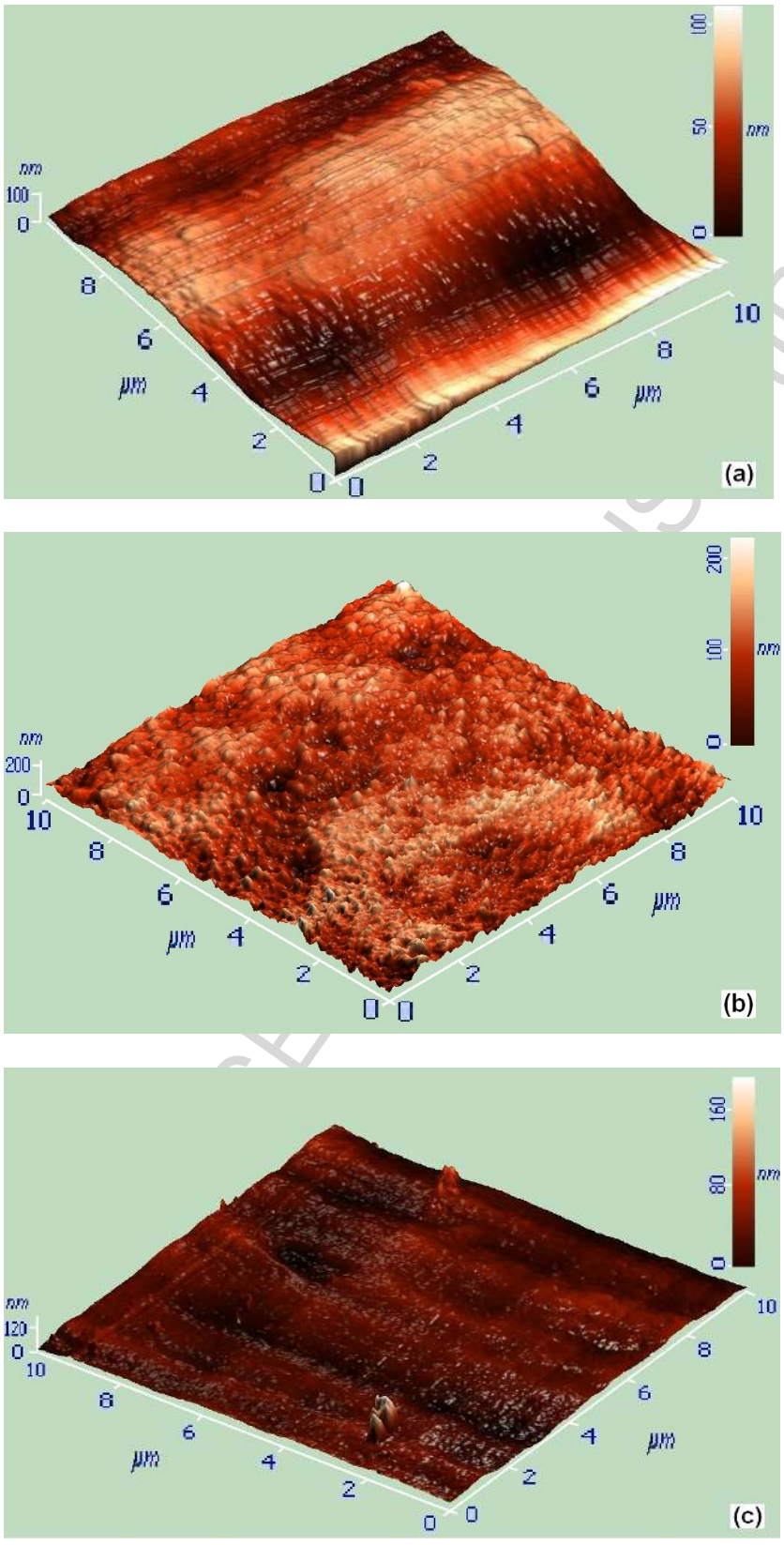

Fig. 2.

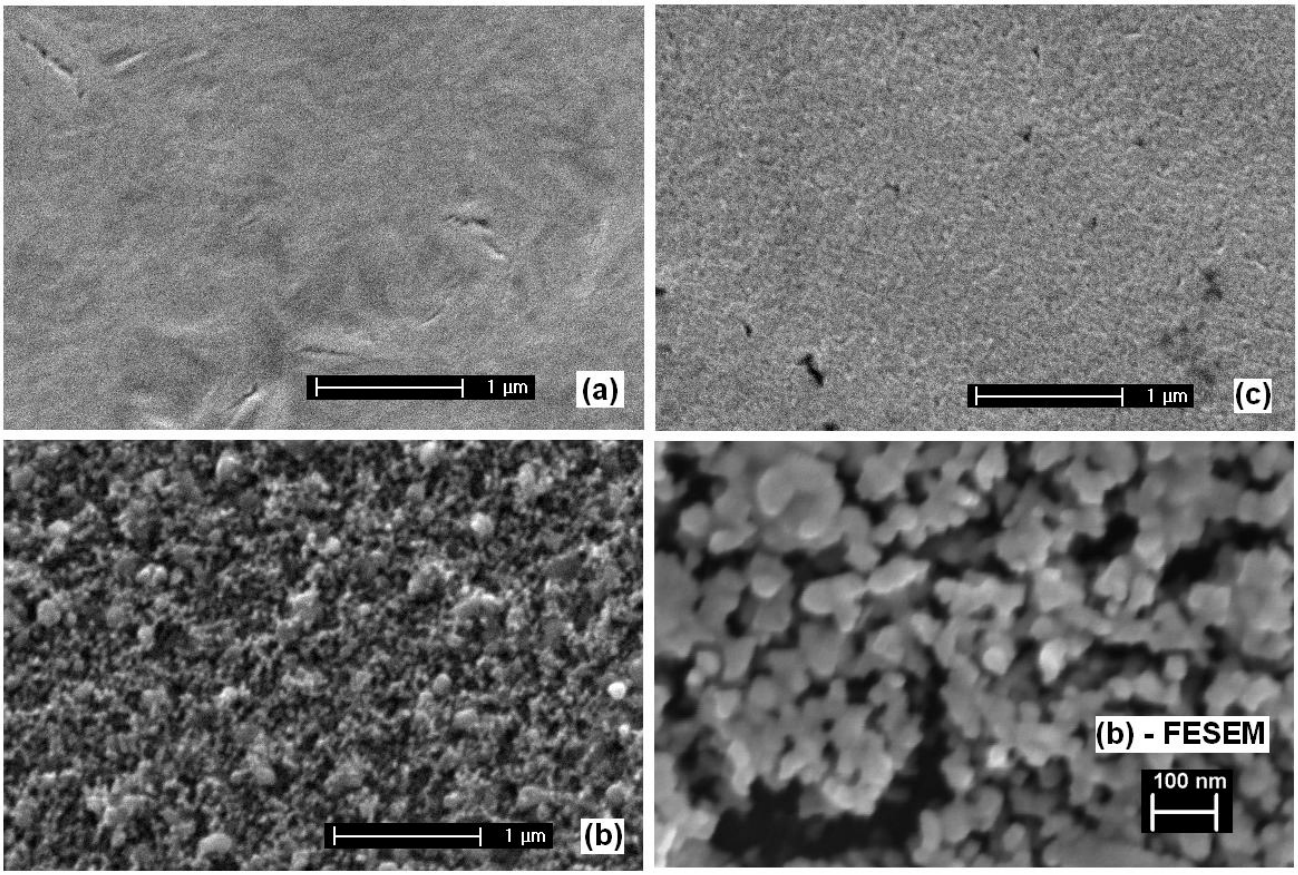

Fig. 3.

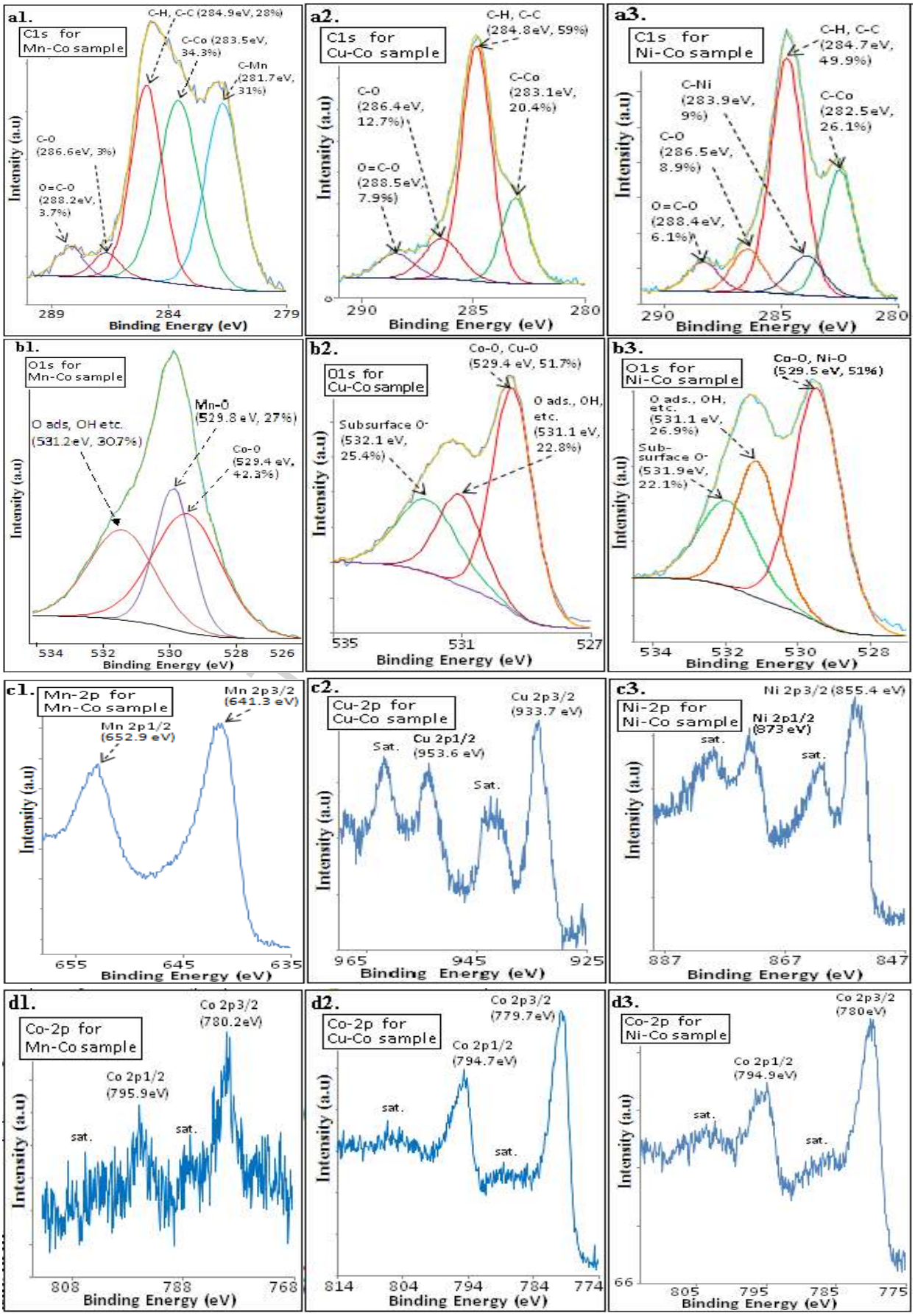

Fig. 4.

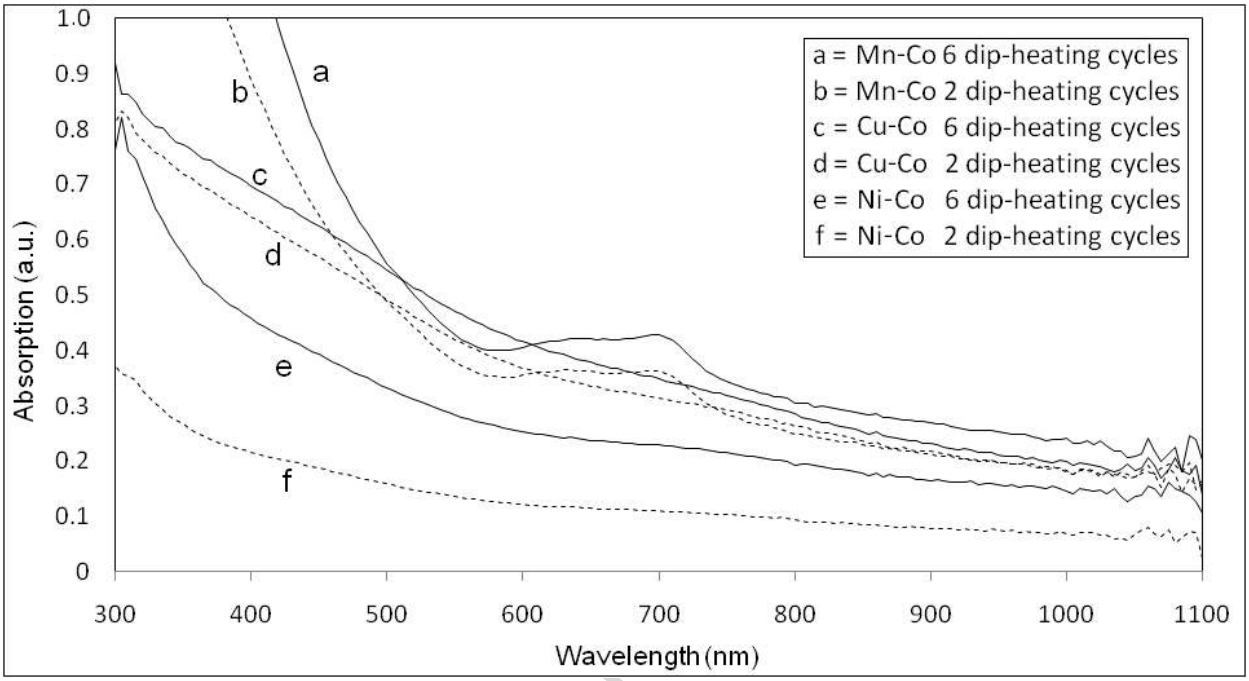

Fig. 5.

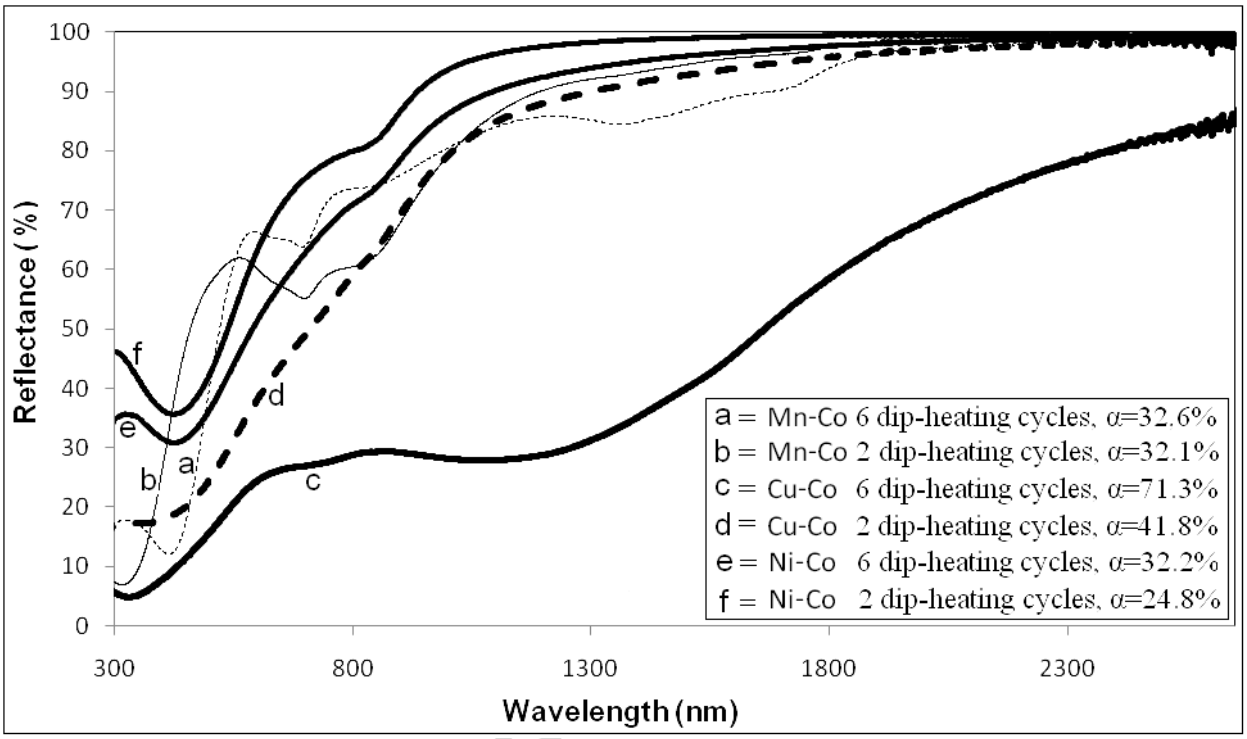

Fig. 6.

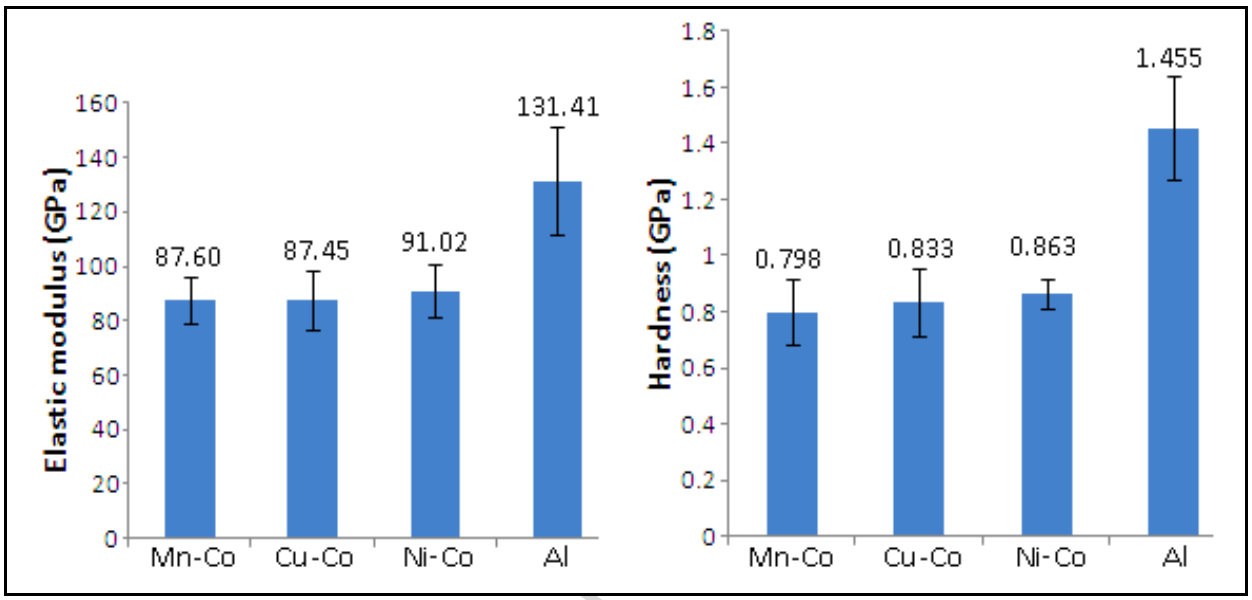

Fig. 7.

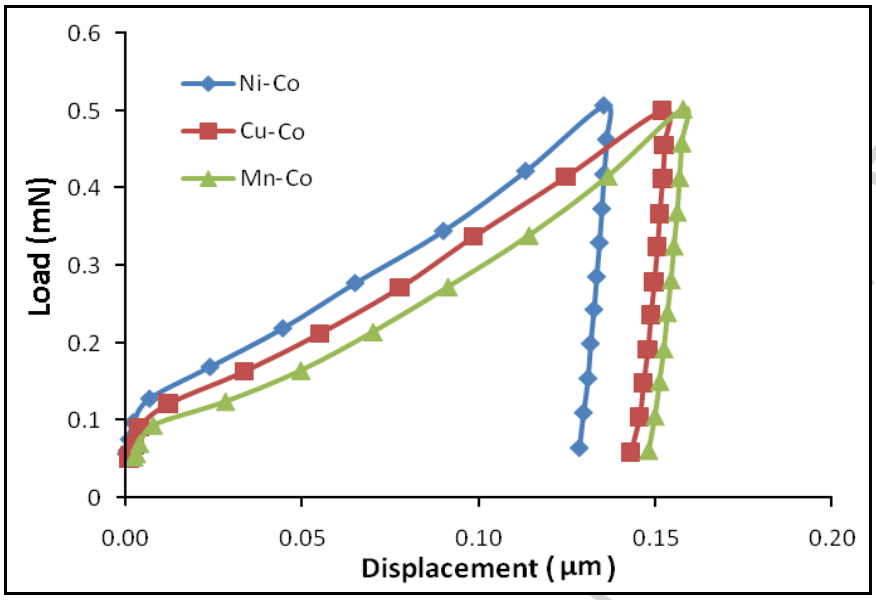

Fig. 8.

Research Highlights

> We synthesize cobalt-based metal oxide thin film coatings. > They are deposited on aluminium and glass substrates via sol-gel dip-coating. > Characterization is via XRD, SEM, AFM and XPS. > Spectrophotometry and Nanoindentation are also conducted. > Copper-cobalt coating exhibits distinctive nano-sized and grain-like morphologies.